Protonation Mechanism of Poly(propylene imine) Dendrimers and Some Associated Oligo Amines

G. J. M. Koper,*,† M. H. P. van Genderen,‡ C. Elissen-Román,‡ M. W. P. L. Baars,‡ E. W. Meijer,‡ and M. Borkovec§

Contribution from the Leiden Institute of Chemistry, Leiden University, Gorlaeus Laboratories, P.O. Box 9502, 2300 RA Leiden, The Netherlands, Laboratory of Organic Chemistry, Eindhoven University of Technology, P.O. Box 513, 5600 MB Eindhoven, The Netherlands, and Federal Institute of Technology, ETH-ITO, Grabenstrasse 3, 8952 Schlieren, Switzerland

Abstract: The protonation behavior of poly(propylene imine) dendrimers and some related oligo amines has been measured using natural abundance ^{15}N-NMR. The chemical shifts of the different *shells* of nitrogen nuclei as a function of pH have been directly interpreted as the degree of protonation for that shell. The thus obtained protonation behavior is described systematically using the Ising model which only requires values for the intrinsic protonation constants and for the pair interaction free energies between the different nitrogen nuclei. This subsequently leads to a quantitative description of the titration curves of the individual shells and to a rationalization of the microscopic and macroscopic equilibrium constants for these molecules.

1. Introduction

Recently, a method has been developed by which the acid–base properties of weak polyelectrolytes and their oligomeric analogs can be quantitatively described.[1–4] Within this *Ising model* one treats the thermal statistics of a collection of interacting sites, which can be either protonated or deprotonated. The basic parameters of the model are microscopic pK values of individual groups and interaction parameters between pairs and possibly triplets of sites. By performing the appropriate thermal average, one obtains the titration curve of the molecule considered. For molecules with a small number of ionizable sites, this leads to the classical description in terms of successive protonation equilibria. Thereby one finds that the ionization constants are expressed in terms of the interaction parameters. For molecules with a large number of sites the titration curves can also be calculated explicitly provided that the structure of the molecule is known as, for example, linear polyelectrolytes.[1,5] The branched structures, such as for instance the industrially very important poly(ethylene imine), are very irregular so that a detailed analysis of these molecules requires additional assumptions.

This, however, is not the case for the novel and highly, albeit very regularly, branched *dendrimers*.[6,7] These dendrimers are built from monomer units with one branch point and a core molecule with one or more branch points. The *first generation* dendrimer consists of the central core molecule with a fixed number of monomers at each branch point, where the core molecule forms the first *shell* and the monomers constitute the second (and last) shell. The second generation dendrimer is synthesized from the first generation dendrimer by again connecting to all branch points the required number of monomers: it then consists of three shells. This procedure can be repeated until further shells cannot be completed because of steric hindrance.

The poly(propylene imine) dendrimers[8] (recently introduced as *Astramol dendrimers*; see Figure 1), as manufactured by DSM (Geleen, The Netherlands), consist of branch points that are also the titratable sites. For the characterization of this type of nitrogen rich dendrimers natural abundance ^{15}N-NMR spectroscopy with inverse gated proton decoupling was used. With this technique one obtains quantitative spectra in which the individual shells of the dendrimer molecules can be identified because all nuclei in one shell are chemically equivalent and because the number of nuclei in one shell differs by a factor of 2 from the previous shell. In chloroform solutions of nitrile terminated dendrimers DAB-*dendr*-(CN)$_x$ with $x = 4, ..., 32$ the resonances of the cyano nitrogens were located at approximately 240 ppm, while the resonances of the tertiary nitrogen nuclei in the interior of the dendrimer were observed in the range 35–40 ppm, where the resonances of the more interior nuclei clearly displayed a more downfield chemical shift.[9] Here, we present the results of natural abundance ^{15}N-NMR spectroscopy on aqueous solutions of amine terminated dendrimers DAB-*dendr*-(NH$_2$)$_x$, with $x = 4, 8, 16$, together with the results of similar measurements on two related oligoamines, NH-(*propyl*-NH$_2$)$_2$ and N-(*propyl*-NH$_2$)$_3$ (see Figure 1). Since the chemical shifts of the nitrogen nuclei are sensitive to protonation, as for instance discussed by Witanowski *et al.*,[10] ^{15}N-NMR provides for a unique method to follow the protonation of the individual shells. Other nuclei, such as ^{1}H and

† Leiden University.
‡ Eindhoven University of Technlogy.
§ Federal Institute of Technology.
⊗ Abstract published in *Advance ACS Abstracts,* July 1, 1997.
(1) Smits, R. G.; Koper, G. J. M.; Mandel, M. *J. Phys. Chem.* **1993**, *97*, 5745–5751.
(2) Borkovec, M.; Koper, G. J. M. *J. Phys. Chem.* **1994**, *98*, 6038–6045.
(3) Borkovec, M.; Rusch, U.; Cernik, M.; Koper, G. J. M.; Westall, J. C. *Colloids Surfaces A* **1996**, *107*, 285–296.
(4) Borkovec, M.; Koper, G. J. M. *Ber. Bunsenges Phys. Chem.* **1996**, *100*, 764–769.
(5) Koper, G. J. M.; Borkovec, M. *J. Chem. Phys.* **1996**, *104*, 4204–4213.
(6) Tomalia, D. A.; Naylor, A. M.; Goddard III, W. A. *Angew. Chem., Int. Ed. Engl.* **1990**, *29*, 138–175.
(7) Frechet, J. M. J. *Science* **1994**, *263*, 1710–1714.

(8) de Brabander-van den Berg, E. M. M.; Meijer, E. W. *Angew. Chem., Int. Ed. Engl.* **1993**, *32*, 1308–1310.
(9) van Genderen, M. H. P.; Baars, M. W. P. L.; van Hest, J. C. M.; de Brabander-van den Berg, E. M. M.; Meijer, E. W. *Recl. Trav. Chim. Pays-Bas.* **1994**, *113*, 573–574.
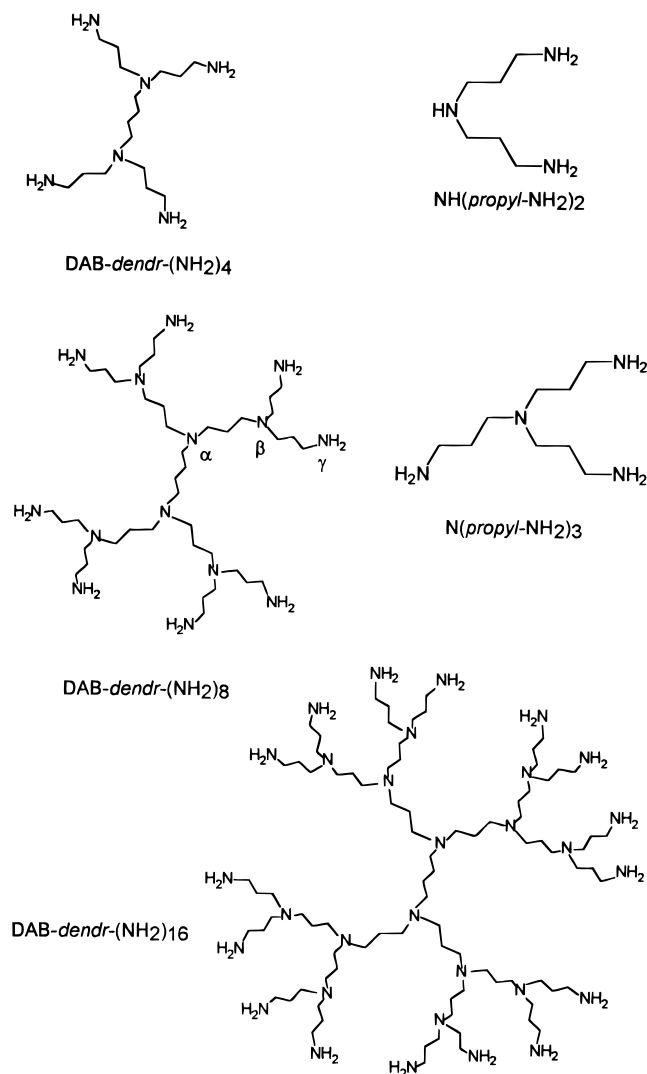(10) Witanowski, M.; Stefaniak, L.; Webb, G. A. *Annu. Rep. NMR Spectrosc.* **1986**, *18*, 1–756.

Figure 1. NH-(*propyl*-NH$_2$)$_2$, formally known as *N,N*-bis(3-amino-propyl)amine, N-(*propyl*-NH$_2$)$_3$, formally known as *N,N,N*-tris(3-aminopropyl)amine, and the three dendrimers DAB-*dendr*-(NH$_2$)$_4$, DAB-*dendr*-(NH$_2$)$_8$, and DAB-*dendr*-(NH$_2$)$_{16}$. The Greek symbols, α, β, ..., indicate nuclei in the various shells.

^{13}C, have also been proposed,[11,12] but because the dissociable protons are directly attached to N nuclei in these oligoamines, the ^{15}N chemical shifts are more sensitive to protonation.

The spectra, consisting of a single resonance peak for each shell, have been recorded for various pH values and have subsequently been interpreted as the degree of protonation *per shell* versus proton activity. The resulting curves are very unlike Langmuir adsorption isotherms, and, hence, a single *microscopic* p*K*-value is insufficient to describe them. In the present paper we shall demonstrate that the protonation behavior is adequately described by means of the Ising model using a small set of parameters. This same set of parameters can be used to predict the macroscopic equilibrium constants which are usually obtained experimentally from the potentiometric titration curve.

2. Materials and Methods

The poly(propylene imine) dendrimers were obtained from DSM (Geleen, The Netherlands). They are synthesized, *in bulk*, starting from a 1,4-diaminobutane (DAB) core molecule. A repetitive cycle of Michael additions with acrylonitrile and catalytic hydrogenations with

Table 1. Details of the Samples Used

sample	concn (mol/kg)	equivalence (mol/kg)	scans
NH-(*propyl*-NH$_2$)$_2$	7.6	22.9	100
NH-(*propyl*-NH$_2$)$_3$	5.3	21.3	100
DAB-*dendr*-(NH$_2$)$_4$	3.2	19.0	100–200
DAB-*dendr*-(NH$_2$)$_8$	1.3	18.1	800
DAB-*dendr*-(NH$_2$)$_{16}$	0.6	17.8	1200

H$_2$/Raney-Co produces dendrimers with nitrile end groups, DAB-*dendr*-(CN)$_x$, or with amine end groups, DAB-*dendr*-(NH$_2$)$_x$, where x = 4, 8, 16, 32, 64, or 128 for the successive generations.[8] *N,N*-Bis(3-aminopropyl)amine was purchased from Acros (Pittsburgh, PA). *N,N,N*-tris(3-aminopropyl)amine was obtained from *N,N,N*-tris(2-cyanoethyl)amine[13] by hydrogenation. *N,N,N*-tris(2-cyanoethyl)amine (20 g, 0.113 mol) was dissolved in 150 mL of toluene and transferred to a Parr-reactor vessel. Three grams of Raney-cobalt catalyst suspension in water was decanted, rinsed with methanol (3 times) and toluene (once), and added to the Parr reactor. The solution was purged three times with hydrogen, and 4.4 g ammonia was added. The system was stirred mechanically at 80 bar hydrogen pressure. The temperature was increased stepwise from 30 °C (1 h), 55 °C (1 h), 75 °C (1 h), to 105 °C (24 h). After cooling and releasing the pressure, the catalyst was removed by filtration over diatomaceous earth on a glass filter. Removal of the solvent and distillation afforded pure product as a colorless liquid (9.5 g, bp 99–102 °C at 0.02 mbar). Characterization data (IR, ^{1}H and ^{13}C NMR) agree with data reported in ref 14.

Solutions for NMR were made in demineralized water, using 5 g of dendrimer or oligomer in 5 g of H$_2$O, resulting in concentrations as given in Table 1. However, due to the exponential increase in the number of nitrogen nuclei, the concentration of basic sites remains fairly constant (see Table 1). Samples were prepared and kept under argon. pH measurements were performed with a Schott CG840 instrument using a combination glass electrode (Schott N37A), and the pH was adjusted by stepwise addition of concentrated HCl (16 mol/kg) or concentrated NaOH (between 5 mol/kg and 15 mol/kg).

^{15}N-NMR measurements were performed on a Bruker AM-400 spectrometer at 40.55 MHz with a switcheable pretuned four-nucleus probehead in 5 mm NMR-tubes. The diameter of the insert was 2 mm. A 20 kHz spectral width was used with 64 K data points. A 90° pulse of 7.0 μs and a delay of 60 s were used for the inverse-gated proton-decoupled experiments. This delay is much larger that the T_1-relaxation times of the nitrogens; the spectra are recorded under "fully relaxed" conditions. Generally, more than 100 scans were needed for one spectrum due to the low ^{15}N abundance (less than 0.3%) resulting in rather long measurement times: 2 h for each 100 scans. The field-frequency lock on the spectrometer was obtained with an internal capillary tube containing CD$_3$NO$_2$. Chemical shifts are determined with an external reference of CD$_3$NO$_2$ ($δ$ = 380.23 ppm)[15] and, for convenience, expressed in terms of the, often used, fictitious scale with liquid NH$_3$ at 25 °C as reference ($δ$ = 0 ppm).

3. Results

Figure 2 represents an example of the measured ^{15}N-NMR spectra as a function of pH, this example belonging to the dendrimer DAB-*dendr*-(NH$_2$)$_8$. The spectra show a limited number of resonances compared to the number of nitrogen nuclei in the molecule because all nuclei that, due to symmetry, are indistinguishable contribute to the same resonance. In addition, this allowed the resonances to be assigned unequivocally using the fact that the integrals of the resonances are proportional to the number of contributing nuclei. The presence of only one resonance for multiple nitrogen nuclei, even when the molecule is partially protonated, indicates that all motions and proton exchange processes are fast with respect to the NMR time scale.

(11) Hague, D. N.; Moreton, A. D. *J. Chem. Soc., Perkin Trans.* **1994**, 2, 265–270.

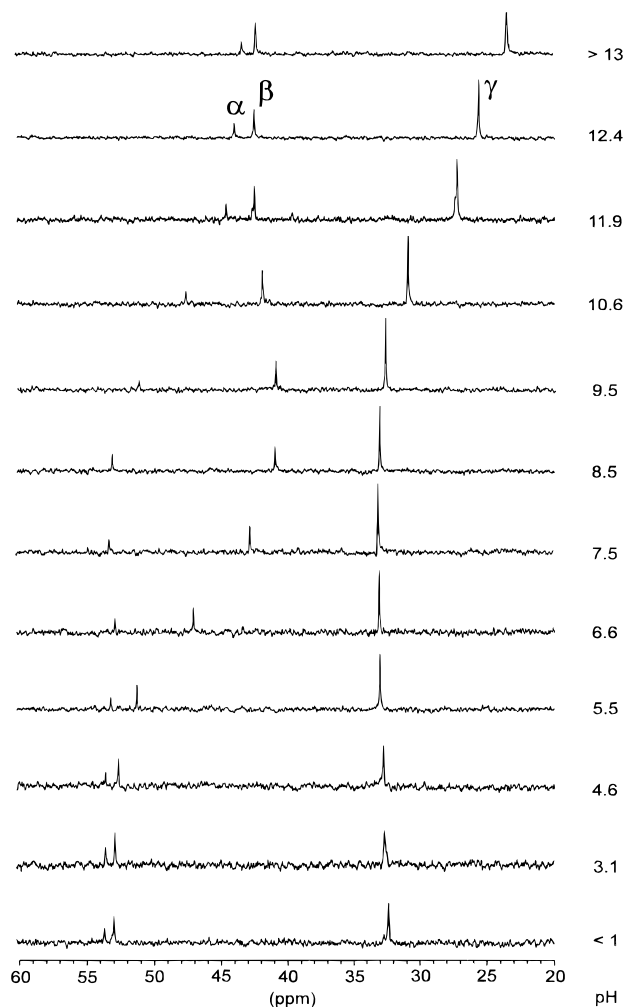(12) Mernissi-Arifi, K.; Schmitt, L.; Schlewer, G.; Spiess, B. *Anal. Chem.* **1995**, *67*, 2567–2574.

(13) Buc, S. R.; Ford, J. H.; Wise, E. C. *J. Am. Chem. Soc.* **1945**, *67*, 92–94.

(14) Dittler-Klingemann, A. M.; Hahn, F. E. *Inorg. Chem.* **1996**, *35*, 1996–1999.

(15) Srinivasan, P. R.; Lichter, R. L. *J. Magn. Reson.* **1977**, *28*, 227–234.

Figure 2. Natural abundance ^{15}N-NMR spectra of the dendrimer DAB-*dendr*-(NH$_2$)$_8$ for different values of the proton concentrations. The greek symbols, α, β, ..., indicate nuclei in the various shells.

The proton activity has been varied from approximately pH 1 to over 11 and the resulting variations in chemical shift have been recorded. The pH values below 2 and over 11 are readings of the pH-meter only and are not reliable. The data points at these extreme pH-values are added to demonstrate the behavior of the investigated molecule under these conditions. Since the pH electrode was calibrated in standard buffer solutions, the high ionic strength (over 1 mol/kg) and the high concentrations of the molecules under investigation will lead to an additional potential difference which will influence the pH values. Therefore, in the range between 2 and 11, the pH values should be read as having an error of ± 0.5 or larger on an absolute scale.

The variation of the chemical shifts with pH have been scaled linearly between 0 and 1, and it is assumed that this variation in chemical shift δ_i corresponds only to the degree of protonation θ_i of the nitrogen nuclei themselves, i.e., to the shell protonation, according to [ref 10, pp 76–77]

$$\delta_i = \delta_i^{(min)}(1 - \theta_i) + \delta_i^{(max)}\theta_i \qquad (1)$$

The minimum and maximum values for the chemical shifts, $\delta_i^{(min)}$ and $\delta_i^{(max)}$ respectively, are given in Table 2. The above equation has also been applied extensively to measure the pH in biosystems.[16]

(16) Stewart, I. M.; Chapman, B. E.; Kirk, K.; Kuchel, P. W.; Lovirc, V. A.; Raftos, J. E. *Biochim. Biophys. Acta* **1986**, *885*, 23–33.

Table 2. Minimum and Maximum Chemical Shift Values Used To Fit NMR-Spectra of the Samples

	α (ppm)	β (ppm)	γ (ppm)	δ (ppm)
NH(*propyl*-NH$_2$)$_2$	39.6–45.4	23.3–33.7		
NH(*propyl*-NH$_2$)$_3$	40.0–52.8	23.4–33.7		
DAB-*dendr*-(NH$_2$)$_4$	42.6–53.3	23.5–33.7		
DAB-*dendr*-(NH$_2$)$_8$	43.0–53.5	40.5–52.8	23.4–33.0	
DAB-*dendr*-(NH$_2$)$_{16}$	43.2–53.5	42.5–52.5	41.0–52.8	24.0–33.1

In the ^{15}N-NMR spectra for the dendrimer DAB-*dendr*-(NH$_2$)$_8$, Figure 2, three resonances are observed: one for the two central tertiary amines, labeled α, that form the inner shell, one for the four tertiary amines, labeled β, that constitute the second shell, and one for the eight primary amines, labeled γ, in the outer shell. The resulting site protonations are shown in Figure 12 and the protonation mechanism will be discussed in the associated paragraph of the next section.

An important observation is that the chemical shift *difference* between the tertiary nitrogen nuclei in shells α and β is virtually identical at both ends of the titration curve (1.1 ppm for pH > 13 and 0.7 ppm for pH < 3.1). This indicates that the protonation state of the primary amines (γ shell) has no influence on the chemical shift of the other nitrogen nuclei. Otherwise, the more nearby located nitrogens in the β-shell would have been more strongly affected. Indeed, the main influence on the nitrogen chemical shift here is the protonation of the site itself, and there is little effect from protonation of nearby sites, contrary to what was suggested by Takeda *et al*. on the basis of their ^{15}N-NMR experiments on thermospermine.[17]

4. Discussion

NH(*propyl*-NH$_2$)$_2$. The first, and simplest, molecule that we shall discuss here is a linear triprotic base NH(*propyl*-NH$_2$)$_2$, i.e., *N,N*-bis(3-aminopropyl)amine. Macroscopically, one discriminates four different protonation states for the molecules: $n = 0$: no bound protons, $n = 1$: one bound proton, $n = 2$: two bound protons, and $n = 3$: three bound protons. The *formation constants* for these protonation states, in terms of the various activities and with respect to the fully deprotonated state, are given by[5]

$$\bar{K}_n = \frac{a_{BH_n}}{a_B a_H^n} \ (n = 1, 2, 3) \qquad (2)$$

and $\bar{K}_0 = 1$ by definition. For each value of the pH $= -\log a_H$, the relative concentration of molecules with n bound protons is given by the *macrostate probabilities* that are, in terms of the formation constants, given by[2]

$$P_n(a_H) = \frac{\bar{K}_n a_H^n}{1 + \bar{K}_1 a_H + \bar{K}_2 a_H^2 + \bar{K}_3 a_H^3} \ (n = 0-3) \qquad (3)$$

(In actual fact, the macrostate probabilities give the relative activities, but, except for protons, we shall assume activity and concentration to be equal in what follows.) The behavior of the macrostate probabilities as a function of pH is depicted in a so called *prevalence diagram*, for NH(*propyl*-NH$_2$)$_2$ such a diagram is shown in Figure 5 (bottom). With these macrostate probabilities one can, for instance, calculate the degree of protonation of the whole molecule which is equal to the number of bound protons over the number of available protonation sites,[2] i.e.,

(17) Takeda, Y.; Samejima, K.; Nagano, K.; Watanabe, M.; Sugeta, H.; Kyogoku, Y. *Eur. J. Biochem.* **1983**, *130*, 383–389.

$$\theta = \frac{1}{3}\sum_{n=0}^{3} nP_n(a_H) \qquad (4)$$

The equilibrium constants for the first, the second, and the last protonation step, which can be found as the ratio of the relevant formation constants, usually have different values. The differences arise from the fact that, in particular, the addition of the last proton requires an additional amount of free energy which is largely due to the electrostatic repulsion with the two already adsorbed protons.[18] In the following we shall rationalize this intuitive argument for the special case of this triprotic molecule using a more microscopic picture of the protonation mechanism. A general exposition is given in the Appendix. In the first place we introduce a labeling procedure for the different *protonation microstates* of a triprotic molecule. To this purpose we define site variables, s_1, s_2, and s_3, that can only have two values: $s_i = 0$ denotes a deprotonated site i and $s_i = 1$ a protonated site i. The eight possible combinations $\{s_1 s_2 s_3\} = \{000, 001, 010, ..., 111\}$ then denote the protonation microstates, see Figure 3. Using the same site variables, the formation free energy of the microstates, relative to the fully deprotonated state, is summarized as[5]

$$F(s_1, s_2, s_3) = -(s_1 + s_3)\mu^{(1)} - s_2\mu^{(2)} + (s_1 s_2 + s_2 s_3)E \quad (5)$$

where $K^{(i)} = \exp(\mu^{(i)}/(kT))$ is the proton affinity of a site of type i. Here, $i = 1$ for a primary amine and $i = 2$ for a secondary amine. Thermal energy is denoted by kT, with k representing the Boltzmann constant and T representing the temperature. E is the additional free energy associated with the repulsive interaction between two (nearest) neighboring protonated sites. We shall also use $\epsilon = E/(kT \ln 10)$, which is the corresponding shift on the pH scale. The above given form of the formation free energy is identical to what in statistical mechanics is known as the Ising hamiltonian.[19] Using the standard analysis techniques for such a model, it follows that the three previously mentioned (macroscopic) formation constants can be expressed in terms of the three new variables, the proton affinities $K^{(1)}$ and $K^{(2)}$ and the proton interaction shift ϵ as[2]

$$\bar{K}_1 = 2K^{(1)} + K^{(2)}$$

$$\bar{K}_2 = 2K^{(1)}K^{(2)}10^{-\epsilon} + (K^{(1)})^2$$

$$\bar{K}_3 = (K^{(1)})^2 K^{(2)} 10^{-2\epsilon} \qquad (6)$$

There are two important facts to be mentioned about the above equations. The first is that the difference between the three formation constants is (*i*) partly due to the electrostatic repulsion and (*ii*) partly an entropic effect due to the degeneracy of the $n = 1$ and the $n = 2$ protonation states: two microstates both contribute equally to these states. Without repulsion, for instance when the protonation sites on the molecule are quite separated from one another, there is still a difference between the equilibrium constants, but this difference is just due to the alternative way of counting the sites: the titration curve is identical to that of a monoprotic base. In addition to rationalizing the set of equilibrium constants and hence the titration curve, the Ising model description also provides for more detailed information about the molecule. In particular, it can
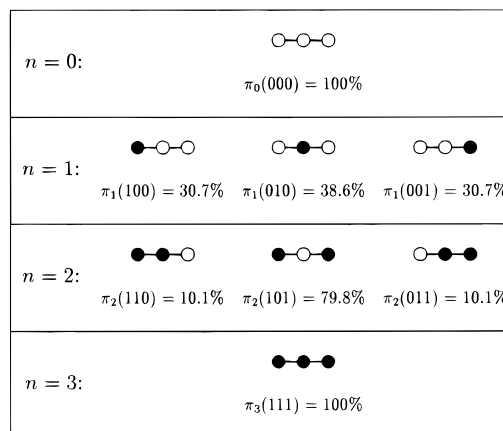
(18) King, E. J. *Acid−Base Equilibria*; Pergamon Press: Oxford, UK, 1965.
(19) Hill, T. L. *An Introduction to Statistical Thermodynamics*; Dover Publ. Inc.: New York, 1986.
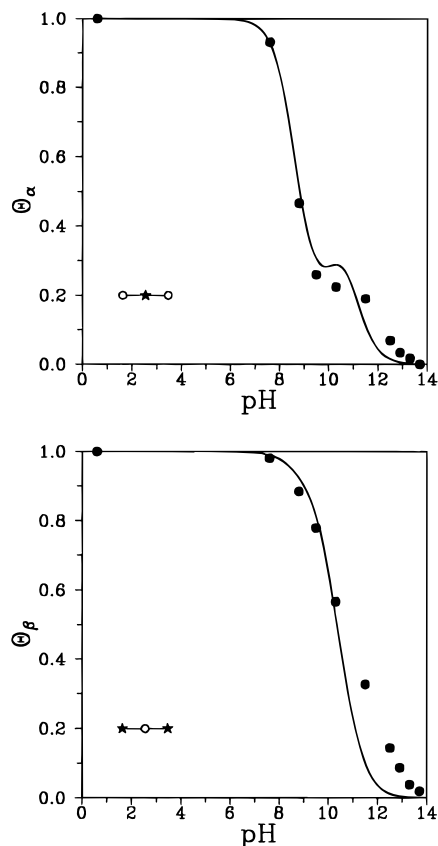(20) Borkovec, M.; Koper, G. J. M. *Langmuir* **1994**, *10*, 2863−2865.

Figure 3. Microstates and conditional microstate probabilities, sorted according to protonation, for NH(*propyl*-NH$_2$)$_2$. The microstates are depicted graphically, a closed circle indicating a protonated site and an open circle a deprotonated site.

be used to calculate the degrees of protonation for the individual sites

$$\theta_j = \sum_{n=0}^{3} A_{jn} P_n(a_H) \qquad (7)$$

which involves the pH-dependent macrostate probabilities and coefficients that only depend on the formation constants, see the Appendix. By fitting these *site degrees of protonation* to the measured ^{15}N-NMR chemical shifts of all molecules we have obtained the parameter values given in Table 3. In the case of NH(*propyl*-NH$_2$)$_2$ there are two resonances to be fit (see Figure 4), one belonging to the central amine and one belonging to the two chemically equivalent terminal amines. The thus obtained parameter values, for the intrinsic pK's of the primary and secondary amines and the pair interaction parameter ϵ_{12} (see Table 3), are subsequently used to calculate the titration curve in Figure 5 (top), the prevalence diagram in Figure 5 (bottom), and the conditional microstate probabilities in Figure 3. These conditional microstate probabilities $\pi_n(s_1 s_2 s_3)$ give the probability of finding a certain configuration $s_1 s_2 s_3$ given that n sites are protonated; they do not depend on pH. Multiplied by the macrostate probability they give the microstate probability, see the Appendix for more details.

Roughly, the titration behavior (Figure 4) can be described as follows: Because the proton affinity of the primary amines is higher than that of the secondary amines, the terminal sites protonate first at low proton concentrations. The difference in affinity between the primary amines and the secondary amine is in the present case not that large, so that the central amine quickly follows. At lower pH the protonation of the central site lags the two terminal sites because of the more favorable microstates where only the terminal sites are protonated: these states have a lower formation free energy due to the absence of a pair interaction energy contribution. At the highest proton concentrations all sites fully protonate.

The titration curve, calculated with the above mentioned fitted parameter values, is given in Figure 5 (top). Although inflection points are visible, there is not much detail in this titration curve. More information is given by the prevalence diagram which is also shown in Figure 5 (bottom). For low values of the pH most of the molecules will be in the $n = 3$ state and for high values of the pH in the $n = 0$ state. Between the last two inflection points in the titration curve, p$K_1 = 11.1$ and p$K_2 = 10.2$, the $n = 1$ state becomes of importance. In this protonation state the two microstates, labeled 001 and 100 where the terminal sites are protonated, are equally probable, albeit slightly

Figure 4. Site degrees of protonation for NH(*propyl*-NH$_2$)$_2$. The symbols represent the experimental points obtained by natural abundance ^{15}N-NMR spectroscopy and the drawn line represents the model predictions using the values in Table 3. The insets show a graph of the molecule; the circles represent the nitrogen nuclei. Asterisks indicate the nuclei being monitored.

Table 3. Parameter Values Used To Fit NMR-Spectra of the Samples

description	parameter	value
intrinsic pK primary amine	p$K^{(1)}$	10.70
intrinsic pK secondary amine	p$K^{(2)}$	10.60
intrinsic pK tertiary amine	p$K^{(3)}$	
α in NH(*propyl*-NH$_2$)$_3$		10.50
α in DAB-*dendr*-(NH$_2$)$_4$		10.40
β and γ in DAB-*dendr*-(NH$_2$)$_8$ and DAB-*dendr*-(NH$_2$)$_{16}$		10.35
α in DAB-*dendr*-(NH$_2$)$_8$ and DAB-*dendr*-(NH$_2$)$_{16}$		9.80
pair interaction across three carbon atoms		
between primary and secundary amines	ϵ_{12}	1.00
between primary and tertiary amines	ϵ_{13}	1.30
between tertiary amines	ϵ_{33}	1.30
pair interaction across four carbon atoms		
between tertiary amines	ϵ'_{33}	0.75

less than the microstate, labeled 010, where the central amine is protonated. This is reflected by the conditional microstate probabilities that are given in Figure 3. The reason for this small difference in microstate probabilities can be traced back to the small difference in proton affinities for the primary and the secondary amines, see Table 3. Between the first two inflection points in the titration curve, pK_2 = 10.2 and pK_3 = 8.6, the n = 2 states becomes of importance. In this protonation state the two microstates, labeled 011 and 110 with one central and one terminal protonated site, are equally probable, this time significantly less than the microstate, labeled 101, where both terminal amines are protonated, see Figure 3. This large difference in microstate probabilities is caused by the large free energy associated with two neighboring protonated sites (gov-
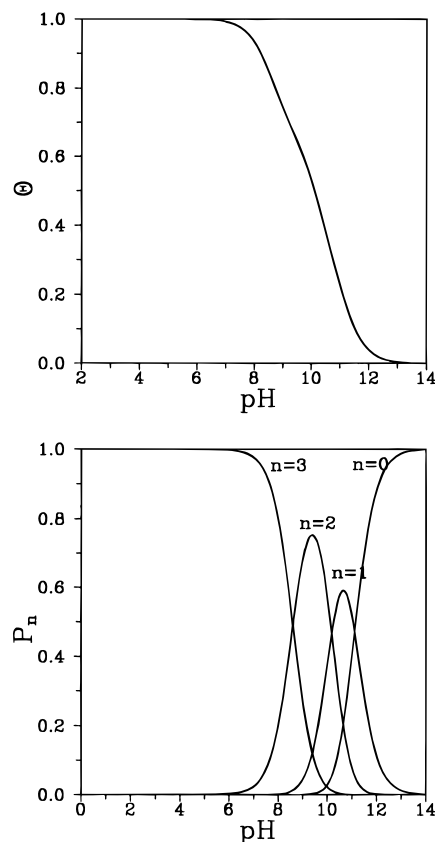

Figure 5. Titration curve (top) and prevalence diagram (bottom) for NH(*propyl*-NH$_2$)$_2$ calculated using the values in Table 3.

erned by ϵ_{12}), which is much larger than the slight differences in proton affinities between the various sites (governed by their intrinsic pK-values).

N(*propyl*-NH$_2$)$_3$. One additional nitrogen added to the previous molecule, which results in N(*propyl*-NH$_2$)$_3$, i.e., *N,N,N*-tris(3-aminopropyl)amine, increases the number of protonation states by one but the number of microstates becomes 16, see Figure 6. Nevertheless, the NMR-spectra only show two resonances because the primary amines are chemically equivalent, see Figure 7. Here and for what follows, it is useful to discriminate *shells* of equivalent nitrogen nuclei. In the present molecule, the internal tertiary amine is the α-shell, and the three primary amines constitute the β-shell. The chemical shifts of the resonances in the NMR-spectra then reflect the degree of protonation of the two shells.

At first glance the protonation mechanism of N(*propyl*-NH$_2$)$_3$ looks rather simple: while increasing the proton concentration first the primary amines in the outer shell protonate only to be followed at much higher proton concentrations by the tertiary amine in the inner shell. The reason for this lies in the unfavorable free energy associated with the formation of three pairs when the tertiary amine is protonated in the presence of three protonated primary amines. The α-shell, however, does show an interesting feature at high pH. This initial protonation at high pH of the inner shell can also be found in the conditional microstate probabilities, Figure 6. In the n = 1 state, all four nuclei are almost equally probable to protonate whereas in the n = 2 and n = 3 states this probability is much less due to the large pair interaction energy. This explains the local maximum in protonation of the α-shell around pH 11. The model predictions for the higher pH-values do not fit well to the NMR-data. Most probably, the readings of the pH-meter do not reflect the actual proton activity due to the alkali error of the glass electrode. Also, at the highest pH-values we observed a phase separation of the sample into a clear and a gel-like phase. This
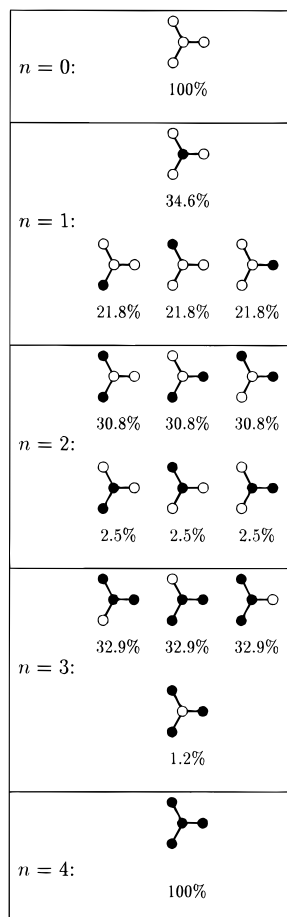
Figure 6. Microstates and conditional microstate probabilities, sorted according to protonation, for N(*propyl*-NH$_2$)$_3$. See Figure 3 for further details.

indicates that the uncharged dendrimers tend to aggregate which hampers the interpretation of the chemical shift as well as the measured pH.

The drawn lines in Figure 7 represent the shell protonations that result from a fit of the model to the experimental NMR-data. The resulting parameter values, the intrinsic pK's for primary and tertiary amines, and the pair interaction parameter ϵ_{13} are given in Table 3. These are subsequently used to obtain the titration curve (top) and the prevalence diagram (bottom) in Figure 8 and the conditional microstate probabilities in Figure 6. In particular the prevalence diagram shows the interesting feature that the $n = 3$ state is rather broad on the pH-scale. From Figure 6 one learns that this state almost exclusively consists of the one microstate where the outer shell is fully protonated. Indeed, further protonation involves protonation of the inner amine which requires three times the pair interaction energy.

DAB-*dendr*-(NH$_2$)$_4$. The smallest dendrimer, DAB-*dendr*-(NH$_2$)$_4$, is very similar to the previous molecule. It has two more nitrogen nuclei so that the number of protonation states increases to 7. The number of microstates increases by a factor 4 to 64, see Figure 9. Again two shells can be discriminated: the two inner nitrogen nuclei, that are connected by a butyl chain, form the α-shell and the four outer nitrogen nuclei constitute the β-shell.

Also the protonation behavior of this dendrimer is very similar to that of the previous molecule, see Figure 10. In particular the initial protonation maximum for the α-shell at low proton concentrations is well reproduced.

The prevalence diagram, Figure 11, is of course more involved than the one for NH(*propyl*-NH$_2$)$_2$ in Figure 8. The
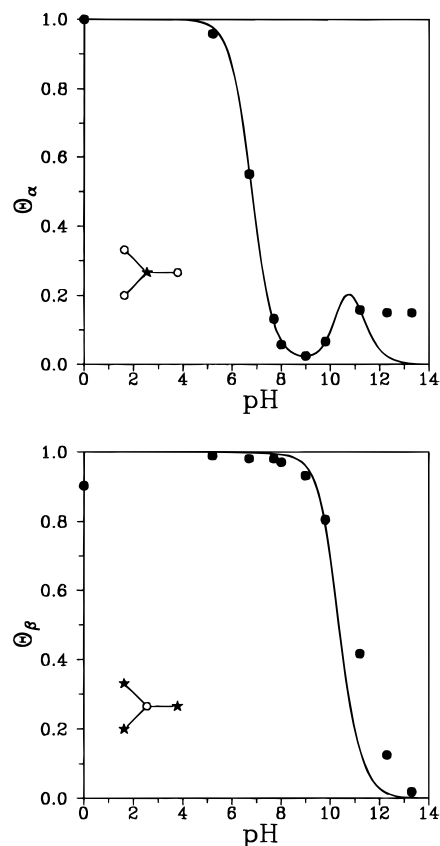

Figure 7. Site degrees of protonation for NH(*propyl*-NH$_2$)$_3$. See Figure 4 for further details.
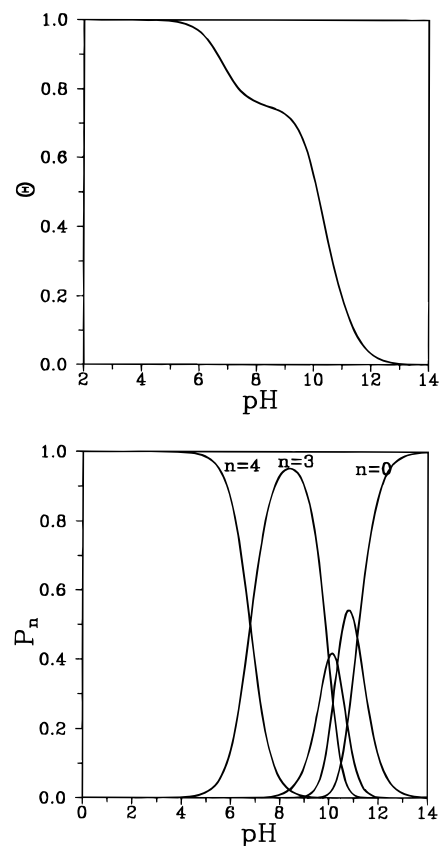

Figure 8. Titration curve (top) and prevalence diagram (bottom) for NH(*propyl*-NH$_2$)$_3$ calculated using the values in Table 3.

extended $n = 3$ state in the previous molecule, where the outer shell is fully protonated, seems not to have a counterpart in the diagram of the present molecule. However, close examination
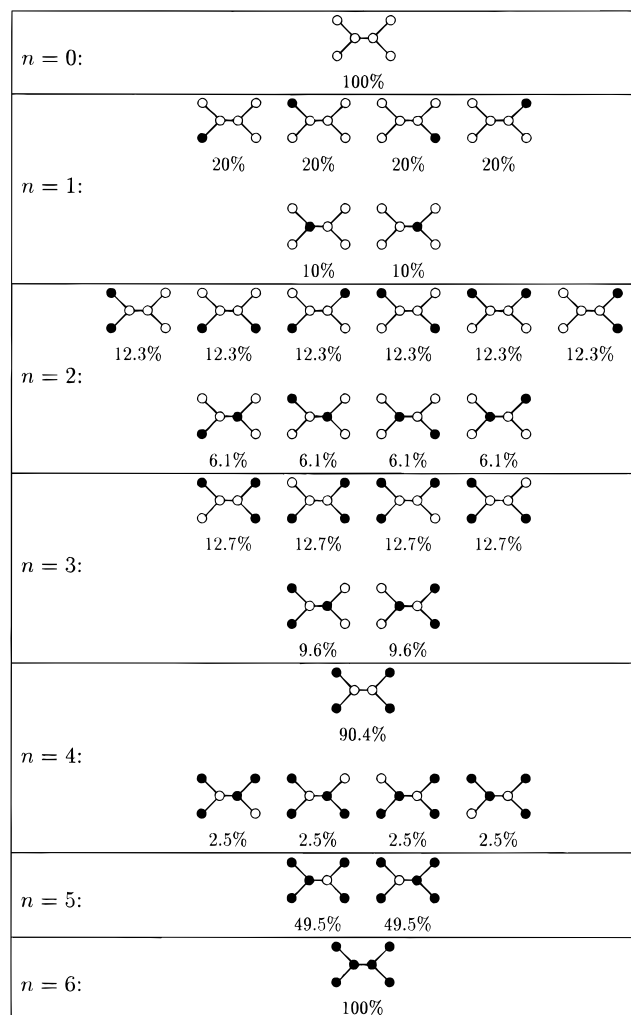
Figure 9. Microstates and conditional microstate probabilities, sorted according to protonation, for DAB-*dendr*-(NH$_2$)$_4$. Only those microstates with probabilities over 0.5% are shown. See Figure 3 for further details.

Figure 10. Site degrees of protonation for DAB-*dendr*-(NH$_2$)$_4$. See Figure 4 for further details.

Figure 11. Titration curve (top) and prevalence diagram (bottom) for DAB-*dendr*-(NH$_2$)$_4$ calculated using the values in Table 3.

of the microstates in Figure 9 and the prevalence diagram in Figure 11 shows that the $n = 4$ state largely consists of the microstate where the outer shell is protonated. Due to the weaker electrostatic interaction across the butyl chain, see Table 3, also microstates with one site of the inner shell protonated contribute significantly (9.1%) to this state. This also makes the titration curve in Figure 11 (top) less structured than for the previous molecule.

DAB-*dendr*-(NH$_2$)$_8$. The three previous molecules all demonstrate a very characteristic two-step protonation behavior that is due to their two-shell structure. The next molecule, DAB-*dendr*-(NH$_2$)$_8$, has a three-shell structure although it essentially protonates in two steps since the odd shells protonate almost simultaneously. The three shell structure is immediately visible from the NMR-spectrum where there are three resonances (see Figure 2) of which the chemical shifts are, as a function of pH, given in Figure 12.

The overall protonation behavior is as follows: first the outer γ-shell and the most inner α-shell protonate with increasing proton concentrations. The middle β-shell follows at lower pH because of its higher formation free energy due to the additional energy of neighboring pairs. The local maximum around pH 11 for the degree of protonation of the β-shell is due to the fact that initially, at low proton concentrations, this shell can protonate simultaneously with the surrounding shells without having neighboring sites protonated. At higher proton concentrations the inner and outer shell are too protonated to avoid
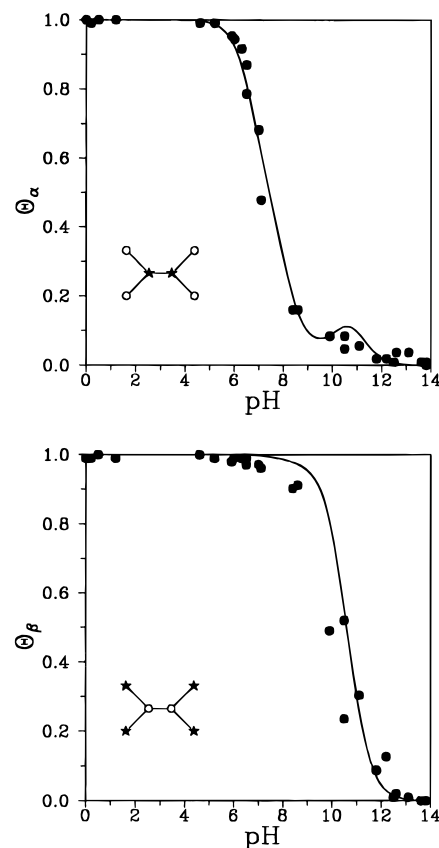
protonated pairs. Around pH 7 there is an interesting local minimum in the degree of protonation of the inner α-shell. This local minimum is most easily explained with the prevalence

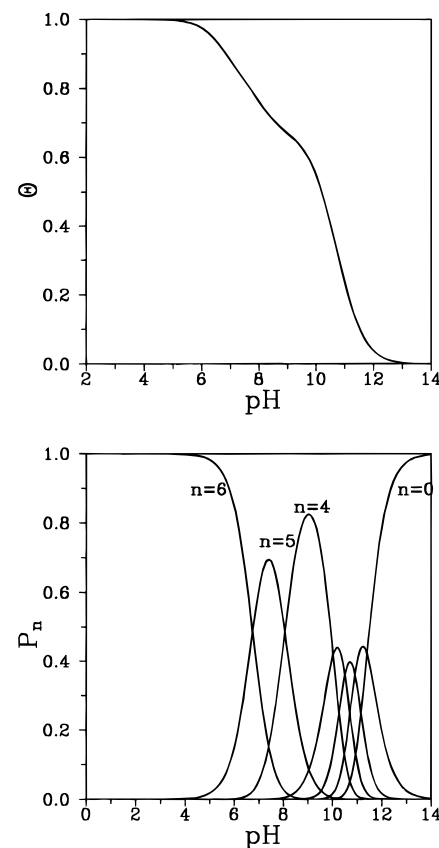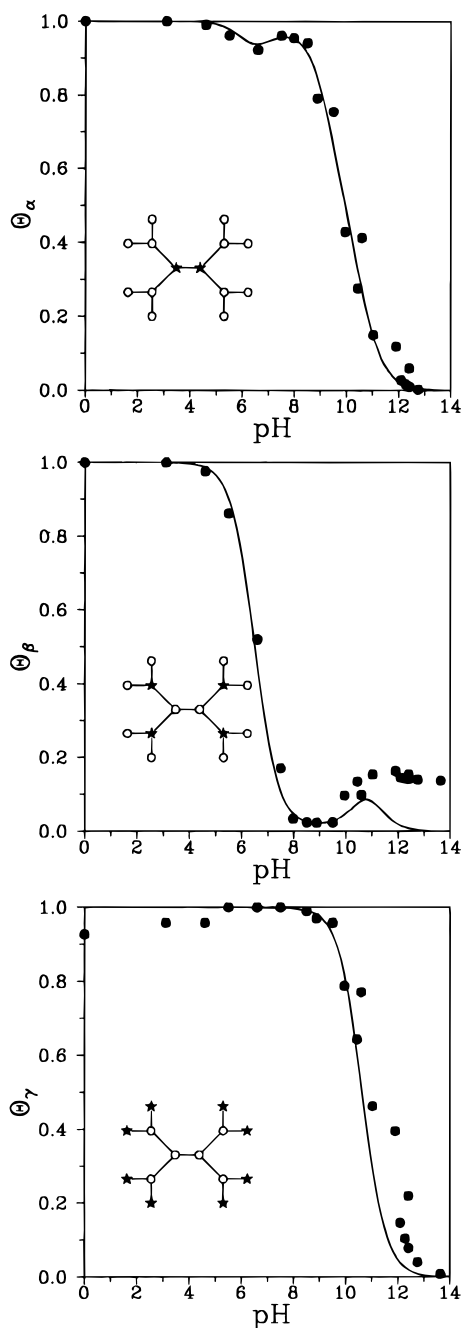**Figure 12.** Site degrees of protonation for DAB-*dendr*-(NH$_2$)$_8$. See Figure 4 for further details.

Figure 13. Titration curve (top) and prevalence diagram (bottom) for DAB-*dendr*-(NH$_2$)$_8$ calculated using the values in Table 3.

diagram in Figure 13 (bottom). Around pH 8 one finds a very pronounced contribution from the $n = 10$ state. From the conditional microstate probabilities (not shown) one finds that largely this protonation state is formed by the microstate with the inner and outer shells occupied (94%). The following proton has to go to a site in the β-shell. With still filled inner and outer shells, the thus formed microstates have a relative probability of 86%. However, there are also microstates with two protons in the β-shell and only one in the inner α-shell. The formation free energy of these microstates is higher than the previously mentioned microstates but still not too much so that the relative probability of this state amounts to approximately 10%. Further protonation finally results in full protonation of the inner shell and this explains the dip in the degree of protonation of the α-shell.

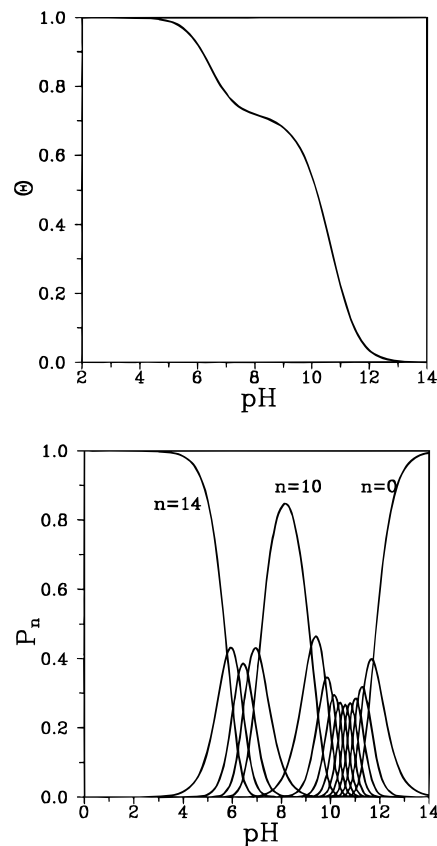The titration curve in Figure 13 (top) reflects a two-step behavior: first the inner and the outer shells protonate, leading to a plateau at roughly 2/3, to be followed by the remaining shells at much lower pH due to the free energy difference of 3ϵ.

DAB-*dendr*-(NH$_2$)$_{16}$. The largest dendrimer that has been measured is DAB-*dendr*-(NH$_2$)$_{16}$, which has four shells and hence shows, sometimes barely detectable, four resonances of which the chemical shifts are, as a function of pH, given in Figure 14.

The protonation behavior is very intricate but, as will be discussed below, does not show any features not revealed in the previously discussed molecules. Starting at low proton concentrations all shells, except for the middle β-shell, protonate slightly. The β-shell, that consists of tertiary amines coordinated with three other tertiary amines, appears to have a lower proton affinity, see Table 3. The outer δ-shell is the first to fully protonate which is explained by the highest proton affinity. The inner α shell initially starts to follow with increasing proton concentration, but around pH 9.5 the β-shell catches up because it can accommodate four more protons while not forming pairs with neighboring sites. Around pH 8 the preferred microstate has the outer δ-shell and the middle β-shell filled, but there are microstates where one of the two sites in the innermost α-shell are protonated. At higher proton concentrations the γ-shell starts to protonate and initially the degree of protonation of the β-shell drops to avoid too many neighboring protonated sites. This also favors a fuller protonation of the α-shell. At very low pH all shells fully protonate.

The local maximum in the degree of protonation of the γ-shell around pH 11 is similar to the local maxima for the other molecules. The interchange between the α and the β shell when the γ-shell protonates is largely due to the weaker pair interaction between the two α sites compared to all the other pair interactions, see Table 3. In fact this behavior is quite similar to the dip in the degree of protonation of the α-shell for the previous molecule DAB-*dendr*-(NH$_2$)$_8$.
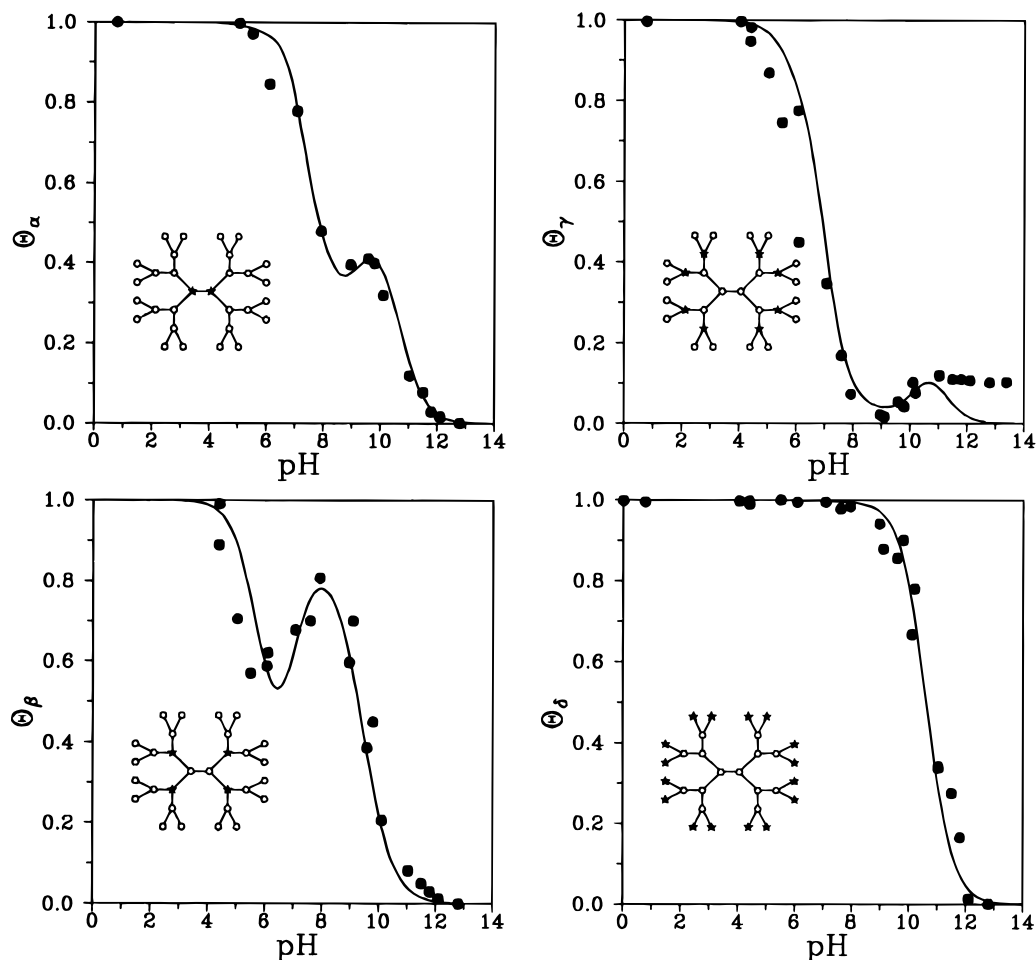
Figure 14. Site degrees of protonation for DAB-*dendr*-(NH$_2$)$_{16}$. See Figure 4 for further details.

5. Conclusions

It has been demonstrated how to describe the protonation behavior of poly(propylene imine) dendrimers and some related oligomers using the Ising model.[20,4] The model requires a very limited set of parameters, site protonation constants and pair interaction free energies, that can subsequently be used for a rationalization of the microscopic and macroscopic equilibrium constants for all the measured molecules.

Natural abundance ^{15}N-NMR has been used, and the chemical shift of the individual nitrogen nuclei has been directly interpreted as the shell protonations. From the quite reasonable agreement between measured and calculated curves one may conclude that this interpretation is correct and that there is little influence from the protonation of nearby sites. There appear to be some subtle differences between the model predictions and the NMR-data. One way to improve the model would be to take into account longer ranged pair and triplet interactions. Because of the high concentrations, intermolecular interactions are also expected to play a role, and these would have to be investigated first before a more elaborate model is proposed.

An important feature that is demonstrated here is that the resulting shell protonation curves are, in general, very unlike Langmuir adsorption isotherms and that, hence, a single *microscopic* p*K*-value is insufficient to describe them.

It is interesting to remark that the characteristic two-step protonation behavior of linear polyelectrolyte[4] is also found for the overall protonation of the dendrimers. In both cases, the short range interaction free energy is responsible for this phenomenon. Here, the phenomenon is directly visible from the shell protonations: first the odd shells protonate followed by the even shells. The difference in geometry causes the linear

polyelectrolytes to plateau at half protonation, whereas the dendrimers plateau around 2/3. Also, the width of the plateau for the linear polyelectrolytes is 2ϵ and for dendrimers it is 3ϵ.

Appendix

The different protonation microstates of a given *N*-functional molecule are fully determined by the string $s_1 s_2 ... s_N$ consisting of variables s_i, one for each distinct protonation site i ($i = 1...N$). These variables are two-valued only, i.e., $s_i = 1$ when the site is protonated and $s_i = 0$ when the site is deprotonated. Also the *free energy of formation*, $F(s_1 s_2 ... s_N)$, of a given microstate, with respect to the fully deprotonated state, is well defined. This free energy of formation, in turn, gives the probability of finding molecules in the particular microstate. It is given by[5]

$$p(s_1 s_2 ... s_N) = \frac{a_H^n \exp\{-F(s_1 s_2 ... s_N)/kT\}}{\Xi} \qquad \text{(A.1)}$$

with k representing the Boltzmann constant, T absolute temperature, and Ξ a normalization constant. The latter normalization constant has the form of a partition function[2,5]

$$\Xi = \sum_{\{s_1 s_2 ... s_N\}} a_H^n \exp\{-F(s_1 s_2 ... s_N)/kT\} \qquad \text{(A.2)}$$

The influence of pH is reflected by the proton activity a_H, which

has a multiplicity that is equivalent to the number of protons involved, i.e., $n = \sum_{i=1}^{N} s_i$.

Prediction of these microstate probabilities requires detailed knowledge of the free energy of formation for the individual protonation microstates. It has been shown that this free energy can be written as the rapidly converging expansion[1,2]

$$\frac{F(s_1 s_2 ... s_N)}{kT \ln 10} = -\sum_{i=1}^{N} pK_i s_i + \sum_{1 \le i < j \le N} \epsilon_{ij} s_i s_j + ... \quad (A.3)$$

The important parameters in this expression are the $pK_i = \log K_i$ with K_i representing the *intrinsic* affinity constant associated with the protonation of the site i, while all remaining sites are deprotonated, and the ϵ_{ij} which are pK-shifts associated with interactions between nearest neighbor pairs of protonation sites.[2,5] Usually, the number of parameters that is necessary for a sufficiently accurate description of the system is much less than the number of different free energies of formation. Moreover, one set of the above mentioned parameters enables a rationalization of the titration behavior of entire classes of molecules.

The conventionally used macroscopic formation constants, or *macroconstants*, can be expressed as the sum of the free energies of formation of the relevant microstates, i.e.,

$$\bar{K}_n = \sum_{\{s_1 ... s_N\}} \delta_{n, \sum_{i=1}^{N} s_i} \exp\{-F(s_1 s_2 ... s_N)/kT\} \quad (A.4)$$

where the Kronecker delta in the summand selects those microstates that have the required number of protonated sites. A special role in the following is played by the macrostate probabilities

$$P_n(a_H) = \frac{\bar{K}_n a_H^n}{\sum_{n=0}^{N} \bar{K}_n a_H^n} \quad (A.5)$$

where the normalization constant is the partition function A.2 that can, alternatively, be expressed as

$$\Xi = \sum_{n=0}^{N} \bar{K}_n a_H^n \quad (A.6)$$

The importance of these macrostate probabilities becomes clear when we express the microstate probabilities (A.1) in terms of the associated macrostate probabilities

$$p(s_1 s_2 ... s_N) = \pi_n(s_1 s_2 ... s_N) P_n(a_H) \quad (A.7)$$

where n again equals the number of protonated sites in the microstate, i.e., $n = \sum_{i=1}^{N} s_i$. While the macrostate probability, $P_n(a_H)$, is pH-dependent, the conditional probability, $\pi_n(s_1 s_2 ... s_N)$, that gives the probability of the microstate $s_1 s_2 ... s_N$ provided that n sites are protonated, is independent of pH. These conditional probabilities turn out only to depend on the free energies of formation, i.e.,

$$\pi_n(s_1 s_2 ... s_N) = \frac{\exp\{-F(s_1 s_2 ... s_N)/kT\}}{\bar{K}_n} \quad (A.8)$$

With the microstate probabilities all macroscopic quantities can be calculated. The protonation degree of site j is given by

$$\theta_j = \frac{1}{N} \sum_{s_1 s_2 ... s_N} s_j p(s_1 s_2 ... s_N) \quad (A.9)$$

and can alternatively be expressed as in eq 7 (particularized to the case of $N = 3$) where the coefficients are independent of pH as is demonstrated by their explicit expression

$$A_{jn} = \sum_{s_1 s_2 ... s_N} s_j \pi_n(s_1 s_2 ... s_N) \delta_{n, \sum_{i=1}^{N} s_i} \quad (A.10)$$

Using the site protonations the overall titration curve can be calculated as

$$\theta = \frac{1}{N} \sum_{j=1}^{N} \theta_j \quad (A.11)$$

which corresponds to eq 4 for the case of $N = 3$.